Journal of Materials Science: Materials in Electronics (2019) 30:9540–9546
https://doi.org/10.1007/s10854-019-01287-z

A $Pb(Zr,Ti)O_3$–$Pb(Zn_{1/3}Nb_{2/3})O_3$–$Bi(Mn_{2/3}Sb_{1/3})O_3$ quaternary solid solution ceramic with low sintering temperature, high piezoelectric coefficient and large mechanical quality factor

Tingwei Huang[1] · Jian Fu[1] · Ruzhong Zuo[1]

Received: 10 February 2019 / Accepted: 5 April 2019 / Published online: 10 April 2019

Abstract

A quaternary high-power piezoelectric ceramic of $0.9Pb(Zr_xTi_{1-x})O_3$–$0.06Pb(Zn_{1/3}Nb_{2/3})O_3$–$0.04Bi(Mn_{2/3}Sb_{1/3})O_3$ + y mol% Fe_2O_3 (x = 0.45–0.53) was reported to exhibit excellent overall properties of $\varepsilon_{33}^T/\varepsilon_0 = 1615$, $d_{33} = 305$ pC/N, $k_p = 0.56$, $Q_m = 1678$, and $T_c = 302$ °C at x = 0.48 and y = 0.7 as sintered at 1040 °C. The relevant mechanism was ascribed to the combined effect of the formation of a traditional morphotropic phase boundary, the low-temperature sintering and amphoteric role of $Bi(Mn_{2/3}Sb_{1/3})O_3$ and the modification of Fe_2O_3 doping. The results demonstrate that Bi-based complex perovskite $Bi(Mn_{2/3}Sb_{1/3})O_3$ can simultaneously provide soft and hard characteristics similar to traditional $Pb(Mn_{1/3}Sb_{2/3})O_3$ and $Pb(Mn_{1/3}Nb_{2/3})O_3$. The addition of a small amount of Fe_3O_3 was found to have an obvious effect on the densification behavior and grain growth, and to simultaneously promote the piezoelectric properties and quality factor Q_m as y < 0.9. Compared with traditional piezoelectric ceramics, low-sintering temperature and excellent piezoelectric properties indicate that the studied composition in current work could have potentials for low-cost high-power device applications.

1 Introduction

High-power piezoelectric ceramics have been widely used in ultrasonic motors and ceramic transformers and so on, where both large piezoelectric coefficients (d_{33}), large electromechanical coupling factors (k_p) and high mechanical quality factors (Q_m) are simultaneously required. One approach to achieving this is to add acceptor dopants (for example, MnO, CuO and Fe_2O_3) into soft piezoelectric solid solution ceramics in the proximity of a traditional morphotropic phase boundary (MPB) between rhombohedral (R) and tetragonal (T) ferroelectric phases, such as $Pb(Zr,Ti)O_3$–$Pb(Mg_{1/3}Nb_{2/3})O_3$ (PZT–PMN), $Pb(Zr,Ti)O_3$–$Pb(Zn_{1/3}Nb_{2/3})O_3$ (PZT–PZN) and so on [1–3]. Another way is to adopt perovskite solid solutions of PZT–$Pb(Mn_{1/3}Sb_{2/3})O_3$ (PZT–PMnS), PZT–$Pb(Mn_{1/3}Nb_{2/3})O_3$ (PZT–PMnN) and PZT–$Pb(Mn_{1/2}W_{1/2})O_3$ with typical amphoteric characteristics owing to variable valences of Mn ions [4–10]. Unfortunately, sintering temperature is usually higher than 1250 °C in these systems, which should be not beneficial to the multilayer piezoelectric ceramic devices. An efficient decrease of sintering temperature by means of doping sintering aids is generally at the expense of piezoelectric and electromechanical properties [11–13].

Bi-based perovskites usually have relatively low sintering temperature, high Curie temperatures (T_c) and excellent ferroelectric and piezoelectric properties owing to the lone-pair $6s^2$ electronic configuration of Bi^{3+} similar to that of Pb^{2+}, such as $BiFeO_3$ (BF), $BiScO_3$ and $Bi(Mg_{1/2}Ti_{1/2})$, etc., which have been extensively investigated for the application of high-T_c piezoelectric ceramics [14–16]. In reference to PZT–PMnS ceramics [4, 8], 4–5 mol% Bi-based complex perovskite $Bi(Mn_{1/2}Ti_{1/2})O_3$ (BMnT) has been successfully substituted for PZT to form ternary solid solutions with relatively low sintering temperature (~ 1120 °C) and good electrical properties of d_{33} ~ 275 pC/N, $k_p = 0.53$, $Q_m = 1164$ and $\tan\delta = 0.66\%$ [17]. Moreover, the substitution of BMnT for PMnS or PMnN in PZT-based solid solution ceramics also helps decrease the lead content to a certain degree for less pollution to the environment.

As known, PZT–PMnS ceramics prove to have larger potentials than other counterparts in high-power piezoelectric materials in terms of their electrical properties. It is

✉ Ruzhong Zuo
piezolab@hfut.edu.cn

[1] Institute of Electro Ceramics & Devices, School of Materials Science and Engineering, Hefei University of Technology, Hefei 230009, People's Republic of China

thus reasonable to expect PZT–BMnS piezoelectric ceramics with better overall properties than those of PZT–BMnT ceramics. Moreover, PZN was believed to intrinsically have a relatively low sintering temperature and can effectively promote the densification of PZT-based ceramics owing to the eutectic reaction between PbO and ZnO [18]. In current work, a new quaternary solid solution of PZT–PZN–BMnS was designed with a fixed amount of PZN (6 mol%) and BMnS (4 mol%), synthetically considering their effects on sintering temperature, piezoelectric properties and T_c values. A further modification work was carried out by doping a small amount of Fe_2O_3 into the R–T MPB-near compositions for the purpose to obtain a low-temperature firable high-power piezoelectric ceramic with excellent piezoelectric performances. The correlation among the phase structure, sintering behavior, grain morphology and piezoelectric and electromechanical properties was discussed in detail.

2 Experimental procedure

The $0.9Pb(Zr_xTi_{1-x})O_3$–0.06PZN–0.04BMnS ($0.9PZ_xT$–0.06PZN–0.04BMnS) (x = 0.45–0.53) ceramics were fabricated by a conventional solid-state reaction method. Analytic-grade powders Bi_2O_3, PbO, ZrO_2, TiO_2, MnO_2, Sb_2O_3, ZnO (Sinopharm Chemical Reagent Co., Ltd) as raw materials were weighed and ball-milled with partially-stabilized ZrO_2 ball in ethanol for 4 h. The mixture was dried, and then calcined at 850 °C for 2 h. The calcined powders with different Fe_2O_3 contents (y = 0–2 mol %) and 0.5 wt% PVB were re-milled for 6 h. The mixed powders were pressed into disks with 10 mm in diameter. The green compacts were heated at 550 °C for 4 h to burn out the binder, and then sintered at 980–1180 °C for 2 h. In order to prevent the vaporization of Bi and Pb, sample disks were buried in the sacrificial powder of the same composition. Silver paste was painted on both sides of the polished surfaces and subsequently fired at 550 °C for 30 min.

The crystal structure of sintered ceramics was characterized by an X-ray diffractometer (XRD, D/Max-rB; Rigaku, Tokyo, Japan) with Cu Kα radiation. The density of sintered ceramics was measured using the Archimedes method. The dielectric properties were measured in a frequency range of 0.1 kHz–1 MHz using an LCR meter (Agilent E4980A, Santa Clara, CA) in a temperature range of 25–500 °C. The specimens were poled at 150 °C under a dc field of 4 kV/mm for 15 min in a silicone oil bath. After poling, the samples were aged at room temperature for 24 h, and then the quasi-static d_{33} values was measured by a Berlincourt meter (YE2730A, Sinocera, Yangzhou, China). The values of k_p and Q_m were determined by a resonance-antiresonance method with an impedance analyzer (PV70A, Beijing Band ERA Co. Ltd. Beijing, China). For the microstructure observation, the polished samples were thermally etched at 850 °C for 30 min, and then analyzed using a field-emission scanning electron microscope (FE-SEM, SU8020, JEOL, Tokyo, Japan). The polarization versus electric field (P–E) hysteresis loops and strain versus electric field (S–E) curves were measured using a ferroelectric test system (Precision LC, Radiant Technologies Inc., Albuquerque, NM) connected with a laser interferometric vibrometer (SP-S 120, SIOS Meβtechnik GmbH, Germany).

3 Results and discussion

Figure 1a shows the XRD patterns of $0.9PZ_xT$–0.06PZN–0.04BMnS ceramics sintered at their optimum temperatures. It can be seen that a pure perovskite structure without any secondary phases can be observed in the studied composition range. With increasing Zr content, the reflection peaks shift to lower angles, indicating that there is a slight unit cell expansion due to the relatively large ionic radius of Zr^{4+} ions compared with that of Ti^{4+} ions (CN = 6, R_{Zr} = 0.72 Å, R_{Ti} = 0.605 Å) [19]. Moreover, the crystal structure gradually changes from T to R symmetry, as manifested by the variation of $(200)_c$ reflection from a typical $(002)_T/(200)_T$

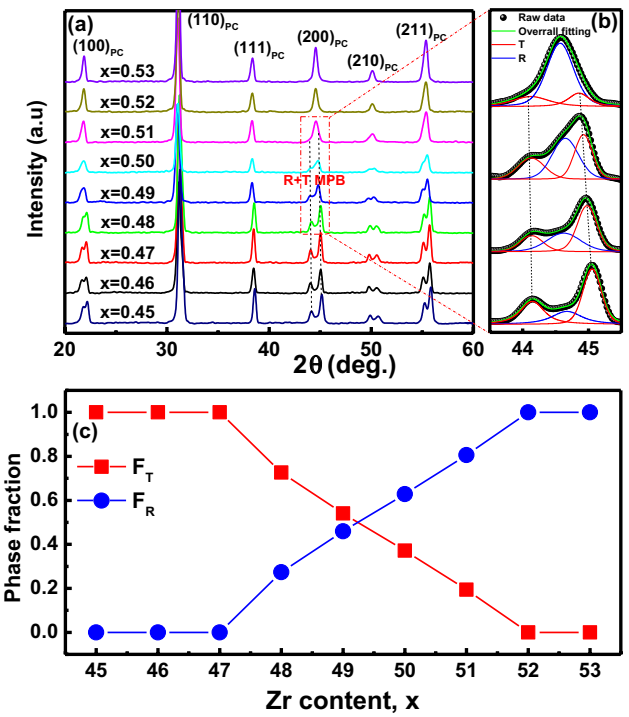

Fig. 1 **a** Room-temperature XRD patterns of $0.9PZ_xT$–0.06PZN–0.04BMnS ceramics sintered at their optimum temperatures, **b** the peak fitting plots of $(200)_c$ reflections for a few representative phase boundary compositions, and **c** the volume fraction of T phase (F_T) and R phase (F_R) changing with x

doublet to a $(200)_R$ singlet. An MPB between R and T phases can be identified in the composition range of x = 0.48–0.51, which can be clearly clarified by the peak fitting of the $(200)_c$ reflection line using the Pseudo-Voigt peak shape function as shown in Fig. 1b. The volume fraction of each phase (F_T and F_R) can be determined by the integrated intensities of $(200)_c$ reflections of R and T phases, as shown in Fig. 1c. It is evident that F_T decreases rapidly from ~ 70% at x = 0.48 to only ~ 20% at x = 0.51 for T phase within MPB.

The dielectric, piezoelectric and electromechanical properties of poled $0.9PZ_xT$–0.06PZN–0.04BMnS ceramics sintered at their optimum temperatures are shown in Fig. 2. It can be seen that $\varepsilon_{33}^T/\varepsilon_0$, d_{33} and k_p values increase firstly with increasing x and reach their maximum with $\varepsilon_{33}^T/\varepsilon_0 = 1450$, $d_{33} = 285$ pC/N, and $k_p = 0.53$ at x = 0.48, which is just located at the T phase rich side within MPB. With further increasing x, these properties show an obvious decrease. By comparison, Q_m shows an opposite tendency with increasing x. It is known that Q_m represents the internal friction in grains [20], which may restrain the domain wall motion. As a result, the observed "softening" behavior indicates that the domain wall motion should be relatively easy within MPB. Although MPB compositions exhibit lower Q_m than both T and R phase compositions, the achieved Q_m value is still as high as 1525 at x = 0.48. The results demonstrate that Bi-based complex perovskite BMnS can simultaneously provide soft and hard characteristics owing to variable valences of Mn ions similar to traditional PMnS and PMnN [4, 6, 8, 11]. The excellent dielectric, piezoelectric properties as well as high Q_m values suggest that this composition may have potentials for high-power piezoelectric device applications. Nevertheless, it is still necessary to make more modification work in order to further reduce sintering temperature and improve its piezoelectric properties.

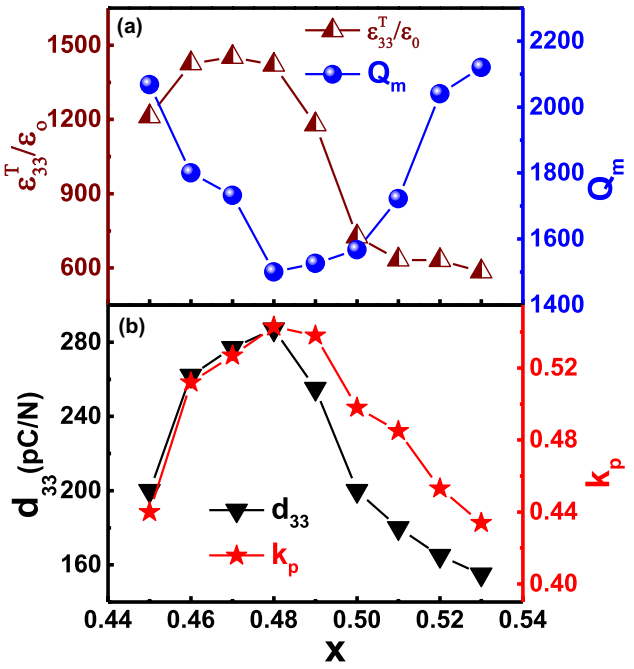

Fig. 2 Various electrical properties of poled $0.9PZ_xT$–0.06PZN–0.04BMnS ceramics sintered at their optimum temperatures

Figure 3 exhibits XRD patterns of $0.9PZ_{0.48}T$–0.06PZN–0.04BMnS ceramics doped with different contents of Fe_2O_3. All ceramics show a pure perovskite structure within the studied doping content, indicating that most of Fe_2O_3 can diffuse into the lattice of the $0.9PZ_{0.48}T$–0.06PZN–0.04BMnS matrix. To clarify the doping effect of Fe_2O_3 on the phase structure, the $(200)_c$ reflection was fitted by Pseudo-Voigt peak shape function, as shown in Fig. 3b. All samples can be well fitted by a coexisting R and T model. Figure 3c shows the variation of lattice parameters and tetragonality c/a. It can be seen that the addition of Fe_2O_3 tends to increase the c/a ratio of the samples due to a slight increase of the cell parameter c but a slight decrease of the cell parameter a. This phenomenon might be correlated with the fact that the addition of BF tends to increase the c/a value of PT [14]. In this study, the doped Fe_2O_3 might form BF in the lattice of Bi-containing perovskites.

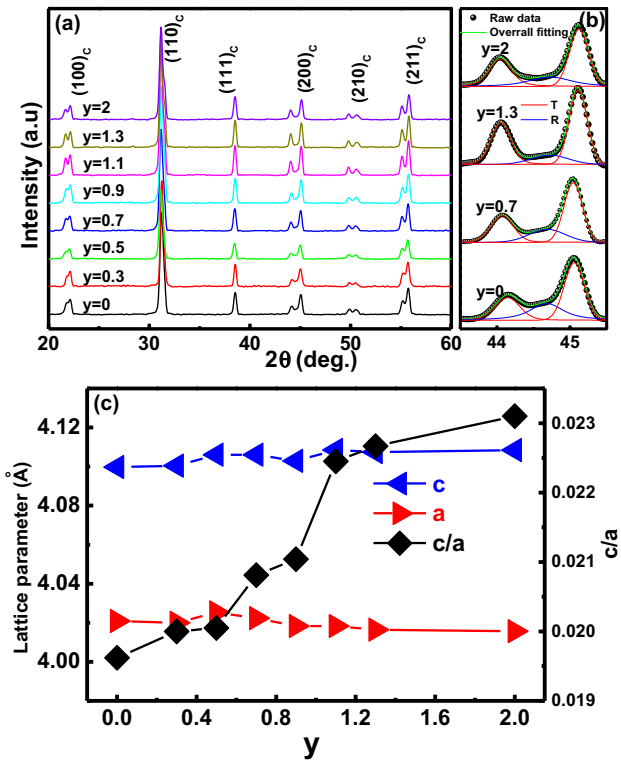

Fig. 3 **a** Room-temperature XRD patterns of $0.9PZ_{0.48}T$–0.06PZN–0.04BMnS+y mol% Fe_2O_3 ceramics sintered at their optimal sintering temperatures, and **b** the peak fitting plots of $(200)_c$ reflections for a few selected compositions, and **c** the variation of lattice parameters and tetragonality c/a as a function of y

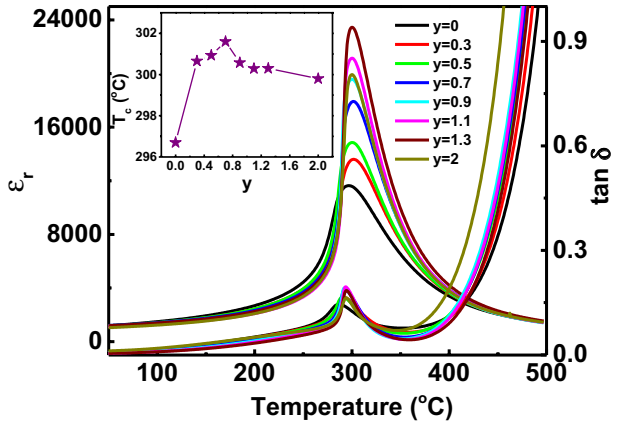

Fig. 4 Temperature dependence of ε_r and tan δ at 1 kHz of $0.9PZ_{0.48}T–0.06PZN–0.04BMnS+y$ mol % Fe_2O_3 ceramics sintered at their optimal temperatures, and the inset shows the variation of T_c with Fe_2O_3 content y

Figure 4 shows the dielectric properties at 1 kHz of $0.9PZ_{0.48}T–0.06PZN–0.04BMnS$ ceramics doped with different Fe_2O_3 contents. It can be seen that the dielectric properties of $0.9PZ_{0.48}T–0.06PZN–0.04BMnS$ ceramics obviously change with varying Fe_2O_3 content. On the one hand, T_c first shows a slight increase with an increase of y and then remains almost constant, as shown in the inset of Fig. 4. The increase of T_c should correspond to the enhancement of the tetragonality c/a shown in Fig. 3c. This is because the increase of tetragonality usually accompanies the enhancement of spontaneous polarization, such that it can sustain a relatively high temperature. Similar trends can be also observed in tanδ–T curves. On the other hand, the addition of a few amount of Fe_2O_3 tends to increase the dielectric maximum value (ε_m) near T_c. Moreover, a relatively broad dielectric peak at y = 0 becomes sharper and sharper with increasing y. This conforms to the fact that the composition with diffuse phase transition exhibits a relatively low ε_m compared with the composition with a typical normal ferroelectric order state. This phenomenon seems to be a common feature in Bi-based relaxor/ferroelectrics, in which polar nanodomains are static with relatively large scales due

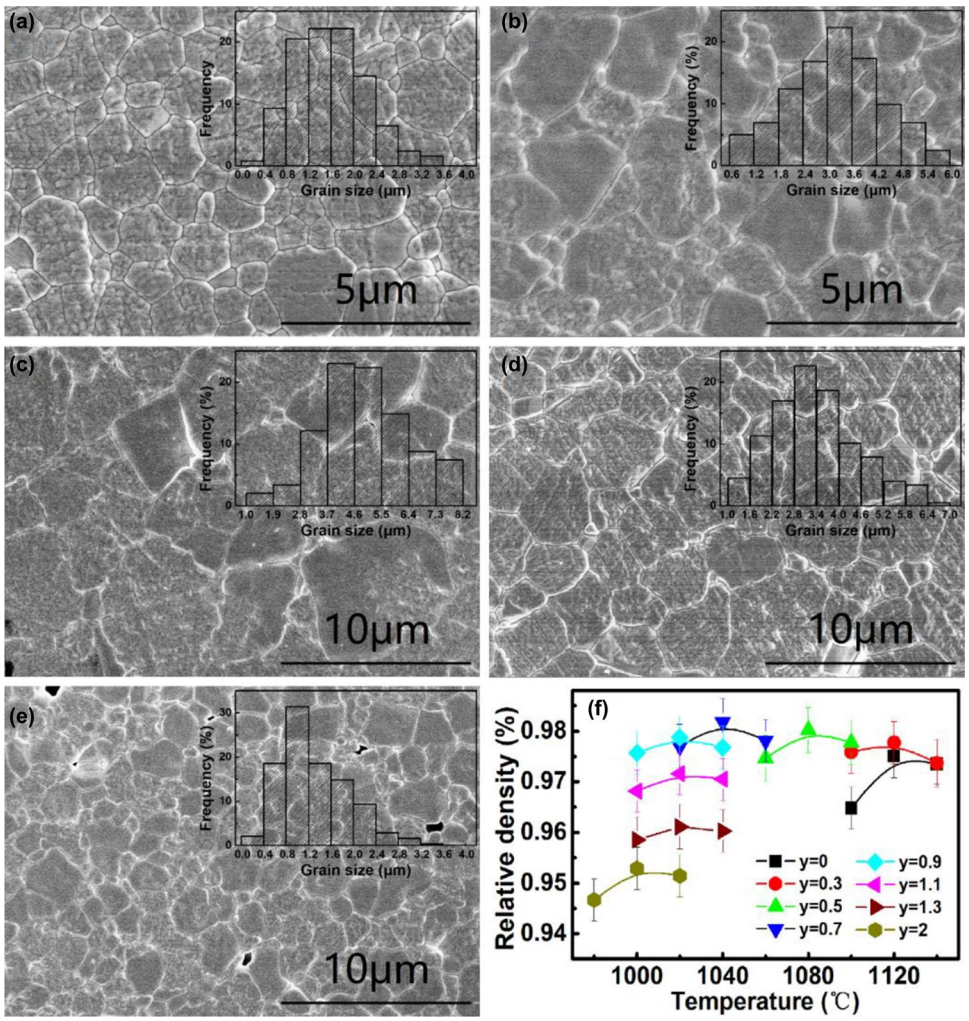

Fig. 5 The SEM images on polished and thermally-etched surfaces of selected $0.9PZ_{0.48}T–0.06PZN–0.04BMnS+y$ mol% Fe_2O_3 ceramics sintered at their optimum temperatures: **a** y = 0 at 1120 °C, **b** y = 0.7 at 1040 °C, **c** y = 0.9 at 1020 °C, **d** y = 1.1 at 1020 °C, **e** y = 2 at 1000 °C and **f** the variation of the relative density as a function of sintering temperature for each composition. The insets of **a**–**e** show the analysis of the grain size distribution

to their high T_c values, and thus make little contribution to the dielectric response [21, 22].

Figure 5a–e shows the SEM images of a few selected compositions sintered at their optimal temperatures. It can be seen that the grain size of the y = 0 sample is relatively uniform with an average size of ~ 1.6 μm. With increasing Fe_2O_3 content, an obvious grain growth can be observed until y = 0.9, simultaneously corresponding to a distinct decrease of the optimal sintering temperature from 1120 °C at y = 0 to 1020 °C at y = 0.9, as shown in the inset of Fig. 5a–e. In addition, the relative density of samples shows a slight increase with increasing Fe_2O_3 content and reaches its maximum value of ~ 98% approximately at y = 0.7–0.9, as shown in Fig. 5f. The influence of Fe_2O_3 doping on the densification and grain growth might be due to the increased lattice distortion caused by the occupation of Fe^{3+} at B-sites. Moreover, low-melting-point BF probably formed during sintering may modify the sintering behavior of the matrix composition and enable it to be densified at a relatively low temperature. However, overmuch Fe_2O_3 tends to degrade the sintering of the samples, leading to a lowered sample density and a reduced grain size through the segregation at the grain boundary. The solubility limit of Fe_2O_3 in the matrix can be also reflected by the fact the c/a value reaches almost constant as y ≥ 1.1.

Figure 6a and b show the composition-dependent P–E hysteresis loops and S–E curves of virgin samples, respectively. Double-like (pinched) P–E loops characterized by a relatively high saturated polarization but a relatively low (or negligible) remanent polarization can be observed in the y = 0 sample. This should be related to the pinning effect of randomly distributed defect dipoles, which tend to remain its virgin direction during polarization switching, resulting in a pinning effect to recover the switched polarization. With increasing Fe_2O_3 content, the pinning effect should be more distinct due to the increased oxygen vacancies. This phenomenon is not distinct in P–E loops but seems to be more pronounced in S–E curves. Most importantly, the y = 0.7–0.9 compositions exhibit a typical sprout-like S–E curves without detectable remanent strain, meaning that the switched polarization can be well recovered after removal of electric field. It should be also noted that the y = 0.7 sample exhibits the largest poling strain (Fig. 6b), suggesting that the lattice and domain contributions should be larger than those in other compositions. This also could induce the enhanced piezoelectric response. However, pinched P–E loops cannot be sustained once y > 0.9 as shown in Fig. 6a. This seems to be related with the weakening of pinning effect of defect dipoles from the solubility limit of Fe_2O_3.

Figure 7 shows various electrical properties for $0.9PZ_{0.48}T$–0.06PZN–0.04BMnS+y mol% Fe_2O_{-3} ceramics sintered at their optimum temperatures. It can be seen that dielectric and piezoelectric properties exhibit a strong composition-dependence although no phase structure change occurs. With increasing Fe_2O_3 content, d_{33}, k_p, $\varepsilon_{33}^T/\varepsilon_0$ and Q_m first exhibit a slight increase, and then reach their maximum values approximately at y = 0.7–0.9, and finally decline rapidly with further increasing y. The change of electrical properties indicates an amphoteric role of doping Fe_2O_3 in $0.9PZ_{0.48}T$–0.04BMS–0.06PZN. The promotion of densification behavior may benefit to piezoelectric properties, in addition to the MPB effect. Furtrhermore, a few amount of Fe_2O_3 might enter the lattice to occupy B-sites, playing a role of acceptor doping and thus enhancing Q_m values by means of pinning domain wall motion, as manifested by Fig. 6. However, as Fe_2O_3 content is beyond 0.8–0.9, nearly all electrical properties exhibit an obvious decrease possibly as a result of the deterioration of the sample densification (Fig. 5). The optimal electrical properties of $\varepsilon_{33}^T/\varepsilon_0 = 1615$, $Q_m = 1678$, $d_{33} = 305$ pC/N, $k_p = 0.56$ and $T_c = 302$ °C can be obtained in 0.7 mol % Fe_2O_3 doped $0.9PZ_{0.48}T$–0.06PZN–0.04BMnS ceramics sintered at a low sintering temperature of 1040 °C, exhibiting an obvious amphoteric characteristic with relatively large piezoelectric properties and high Q_m. These features should well satisfy the requirement of high-power piezoelectric devices,

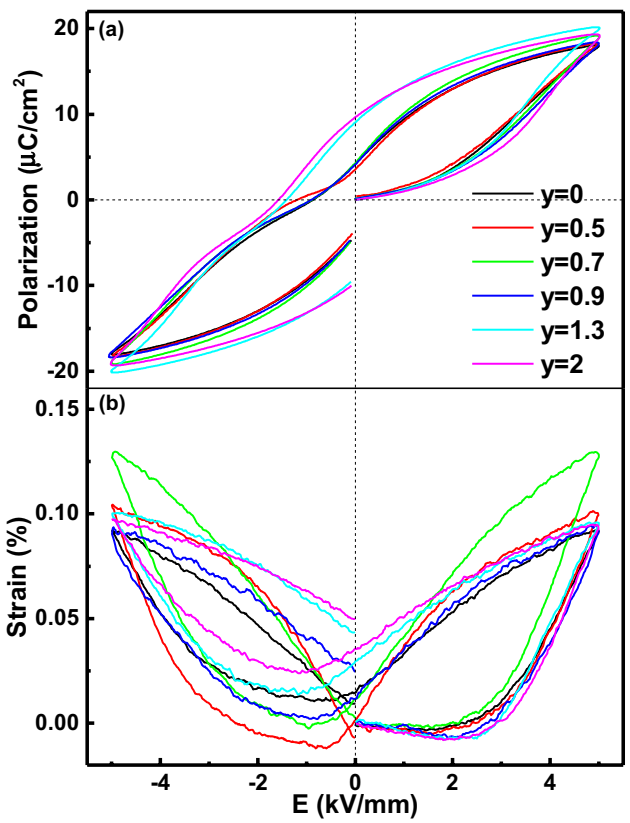

Fig. 6 **a** P–E hysteresis loops and **b** S–E curves of unpoled $0.9PZ_{0.48}T$–0.06PZN–0.04BMnS+y mol% Fe_2O_3 ceramics

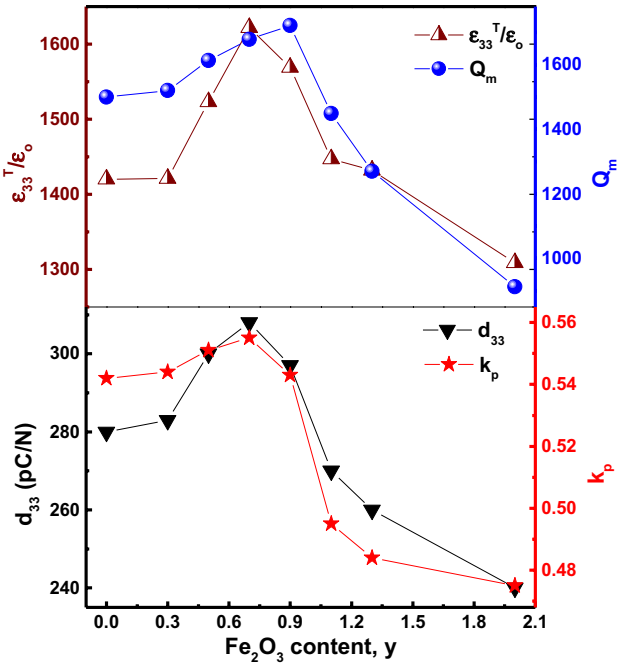

Fig. 7 Various electrical properties of the $0.9PZ_{0.48}T$–0.06PZN–0.04BMnS+y mol% Fe_2O_3 ceramics sintered at their optimum temperatures

particularly low-cost multilayer piezoelectric devices. Table 1 compares the electrical properties of a couple of PZT-based piezoelectric material systems for high-power piezoelectric devices in terms of their sintering temperature and various piezoelectric and electromechanical properties. It can be seen that traditional piezoelectric ceramics reported previously such as PZT–PMnS, PZT–PMnS–PMnN or acceptor doped PZT–PZN/PZT–PMN, are characterized by difficulties in simultaneously achieving low sintering temperature and excellent piezoelectric properties. The addition of sintering aids would effectively decrease sintering temperature but sacrifice the final piezoelectric properties. By comparison, the studied composition exhibits excellent overall properties by taking advantages of the composition's own characteristics, showing large potentials for high-power device applications.

4 Conclusions

A quaternary high-power $0.9PZ_xT$–0.06PZN–0.04BMnS+y mol% Fe_2O_3 solid-solution piezoelectric ceramic was investigated in terms of the phase structure, sintering behavior and microstructure and various electrical properties. It is found that Bi-based complex perovskite BMnS can simultaneously provide soft and hard characteristics owing to variable valences of Mn ions similar to traditional PMnS and PMnN. Moreover, the addition of a small amount of Fe_2O_3 can promote the densification behavior, grain growth and modify piezoelectric and electromechanical properties, exhibiting a simultaneous promotion role of piezoelectric properties (d_{33} and k_p) and quality factor Q_m within $y < 0.9$ owing to both improved sample density and enhanced pinning effect of domain wall motion. The excellent overall properties of $\varepsilon_{33}^T/\varepsilon_0 = 1615$, $d_{33} = 305$ pC/N, $k_p = 0.56$, $Q_m = 1678$, and $T_c = 302$ °C at $x = 0.48$ and $y = 0.7$ as sintered at 1040 °C, which is far below that of traditional PZT-based high-power piezoelectric ceramics. Compared with traditional piezoelectric ceramics, low-sintering temperature and excellent piezoelectric properties indicate that the studied composition in current

Table 1 The comparison between high-power traditional piezoelectric ceramics and the currently studied system (T_S denotes the sintering temperature)

Compounds	Dopants	T_S (°C)	$\varepsilon_{33}^T/\varepsilon_0$	d_{33} (pC/N)	k_p	Q_m	T_C (°C)	Ref.
$0.4Pb(Mg_{1/3}Nb_{2/3})O_3$–$0.25PbZrO_3$–$0.35PbTiO_3$	MnO_2	1150	723	177		949	215	[1]
$Pb[(Zr_{0.52}Ti_{0.48})_{0.85}(Mg_{1/3}Nb_{2/3})_{0.02}(Zn_{1/3}Nb_{2/3})_{0.13}]O_3$	CuO	920	982	280	0.53	1645		[23]
$0.9(Pb_{0.94}Sr_{0.06})(Zr_{0.51}Ti_{0.49})O_3$–$0.1Pb(Mn_{1/3}Nb_{2/3})O_3$		1200	1290	274	0.533	800	287	[11]
$Pb[(Mn_{1/3}Nb_{2/3})_{0.06}$–$(Zr_{0.52}Ti_{0.48})_{0.94}]O_3$	PbO CuO	1020	1450	238	0.54	850	348	[24]
$0.05Pb(Mn_{1/3}Sb_{2/3})O_3$–$0.95Pb(Zr_{0.52}Ti_{0.48})O_3$		1240	1540	360	0.58	1210	281	[4]
$0.075Pb(Mn_{1/3}Nb_{2/3})O_3$–$0.125Pb(Zn_{1/3}Nb_{2/3})O_3$–$0.8Pb(Zr_{0.52}Ti_{0.48})O_3$		1200	842	215	0.57	1020	320	[25]
$0.9Pb(Zr_{0.52}Ti_{0.48})O_3$–$0.05Pb(Mn_{1/3}Sb_{2/3})O_3$–$0.05Pb(Zn_{1/3}Nb_{2/3})O_3$	MnO_2 WO_3 ZnO	1120	1100	300	0.55	1899	270	[26]
$0.95Pb(Zr_{0.51}Ti_{0.49})O_3$–$0.05Bi(Mn_{1/2}Ti_{1/2})O_3$		1120	1226	275	0.53	1164	341	[17]
$0.9Pb(Zr_{0.48}Ti_{0.52})O_3$–$0.04Bi(Mn_{2/3}Sb_{1/3})O_3$–$0.06Pb(Zn_{1/3}Nb_{2/3})O_3$	Fe_2O_3	1040	1615	305	0.56	1678	301	This work

work could have potentials for low-cost high-power device applications.

Acknowledgements This work was supported by the National Natural Science Foundation of China (Grant No. 51472069).

References

1. Y.K. Yan, K.H. Cho, S. Priya, J. Am. Ceram. Soc. **94**, 4138 (2011)
2. M.K. Zhu, P.X. Lu, Y.D. Hou, H. Wang, J. Mater. Res. **20**, 2670 (2005)
3. Y.D. Hou, M.K. Zhu, H. Wang, B. Wang, H. Yan, C.S. Tian, Mater. Lett. **58**, 1508 (2004)
4. Z.G. Zhu, G.R. Li, Z.J. Xu, W.Z. Zhang, Q.R. Yin, J. Phys. D Appl. Phys. **38**, 1464 (2005)
5. Z.P. Yang, X.M. Zong, H. Li, Y.F. Chang, Mater. Lett. **59**, 3476 (2005)
6. A. Prasatkhetragarm, R. Yimnirun, Ceram. Int. **39**, S91 (2013)
7. V. Kalem, M. Timucin, J. Eur. Ceram. Soc. **33**, 105 (2013)
8. M. Kobune, H. Okuda, H. Nishioka, T. Kikuchi, Jpn. J. Appl. Phys. **52**, 09KD10 (2013)
9. D.W. Wang, M.S. Cao, Q.L. Zhao, Y. Cui, S.J. Zhang, Phys. Status Solidi R **7**, 221 (2013)
10. Y. Li, D.W. Wang, W.Q. Cao, B. Li, J. Yuan, D.Q. Zhang, S.J. Zhang, M.S. Cao, Ceram. Int. **41**, 9647 (2015)
11. S. Priya, H.W. Kim, K. Uchino, J. Am. Ceram. Soc. **87**, 1907 (2004)
12. C.C. Tsai, S.Y. Chu, C.S. Hong, S.F. Chen, J. Eur. Ceram. Soc. **31**, 2013 (2011)
13. S.Y. Yoo, J.Y. Ha, S.J. Yoon, J.W. Choi, J. Eur. Ceram. Soc. **33**, 1769 (2013)
14. D.I. Woodward, I.M. Reaney, R.E. Eitel, C.A. Randall, J. Appl. Phys. **94**, 3313 (2003)
15. C.A. Randall, R. Eitel, B. Jones, T.R. Shrout, D.I. Woodward, I.M. Reaney, J. Appl. Phys. **95**, 3633 (2004)
16. T.T. Zou, X.H. Wang, H. Wang, C.F. Zhong, L.T. Li, I.W. Chen, Appl. Phys. Lett. **93**, 192913 (2008)
17. B. Zhang, H. Qi, R.Z. Zuo, Ceram. Int. **44**, 5453 (2018)
18. Z. Gui, H. Hu, L. Li, X. Zhang, Solid State Phenom. **25–26**, 309 (1992)
19. R.D. Shannon, Acta Crystallogr. A **32**, 751 (1976)
20. H. Frayssignes, M. Gabbay, G. Fantozzi, N.J. Porch, B.L. Cheng, T.W. Button, J. Eur. Ceram. Soc. **24**, 2989 (2004)
21. J. Fu, R.Z. Zuo, Acta Mater. **61**, 3687 (2013)
22. H.F. Yi, R.Z. Zuo, J. Am. Ceram. Soc. **97**, 1912 (2014)
23. X.L. Chao, D.F. Ma, R. Gu, Z.P. Yang, J. Alloys Compd. **491**, 698 (2010)
24. C.C. Tsai, S.-Y. Chu, C.-H. Lu, I.E.E.E. Trans, Ultrason. Ferroelectr. Freq. Control **56**, 660 (2009)
25. F. Gao, L.H. Cheng, R.Z. Hong, J. Liu, C.J. Wang, C.S. Tian, Ceram. Int. **35**, 1719 (2009)
26. H. Li, Z.P. Yang, L.L. Wei, Y.F. Chang, Mater. Res. Bull. **44**, 638 (2009)